Available online at www.sciencedirect.com
ScienceDirect
Trans. Nonferrous Met. Soc. China 30(2020) 582−594
Transactions of Nonferrous Metals Society of China
www.tnmsc.cn

Effect of solidification process parameters on dry sliding wear behavior of AlNiBi alloy

T. M. BOTELHO[1], H. M. AZEVEDO[1], G. H. MACHADO[1], C. R. BARBOSA[1], F. S. ROCHA[1], T. A. COSTA[1], O. L. ROCHA[1,2]

1. Federal Institute of Education, Science and Technology of Pará, IFPA, Almirante Barroso Avenue 1155, 66093-020 Belém, PA, Brazil;
2. Institute of Technology, Federal University of Pará, UFPA, Augusto Correa Avenue 1, 66075-110 Belém, PA, Brazil

Received 2 August 2019; accepted 26 December 2019

Abstract: As-cast samples of the Al−3wt.%Ni−1wt.%Bi alloy resulting from the horizontal directional solidification process were subjected to the micro-abrasive wear test. The effects of the solidification thermal and microstructural parameters, such as the growth and cooling rates and the cellular and primary dendritic spacings (V_L and T_R; λ_1 and λ_c; respectively), were evaluated in the wear resistance of the investigated alloy. The tribological parameters analyzed were the wear volume and rate (V_w and R_w). The solidification experiments and the wear tests were carried out by means of a water-cooled horizontal directional solidification device and a rotary-fixed ball wear machine, respectively. The results show lower V_w and R_w values correspond to finer microstructures and the V_w dependence on λ_1 is characterized by an experimental mathematical equation. A better distribution of Bi soft droplets and Al_3Ni hard intermetallic particles is observed within the finer interdendritic region and, in consequence, the better wear resistance is achieved in as-cast samples with dendritic morphology rather than cellular morphology. A transition of wear mechanism from adhesive to abrasive is observed.

Key words: unsteady-state horizontal solidification; dry sliding wear; cellular/dendrite arm spacing; microhardness; Bi particle; Al_3Ni particle

1 Introduction

It is very well known that aluminum-based alloys have gained highlight due to their excellent specific strength, especially in the aerospace and automotive industries, since the substitution of components manufactured of heavier alloys by lighter materials in these industries, promotes considerable reductions in the weight of the final product and, as a consequence, increases the energy efficiency of manufactured cars and aircraft, fundamental to market competitiveness. In the particular case of Al−Ni alloys, they have achieved attention due to their high-temperature structural applications, excellent performances in corrosion resistance and high-temperature mechanical properties [1−8].

Studies have reported the influence of thermal and microstructural parameters in solidification on the mechanical [1−3,7,8], electrical and thermal properties [4−6] of binary Al−Ni alloys. These investigations have observed that the typical solidification microstructure is composed of a predominantly dendritic aluminum-rich matrix (α), surrounded by a eutectic mixture within the interdendritic regions, composed of α+β, where β is an intermetallic compound (Al_3Ni), responsible for the increase of mechanical strength of Al−Ni alloys, since the α-phase is soft and ductile. In turn, a third alloying element is added in these alloys, such as Cu and Bi, further improving the mechanical

Corresponding author: O. L. ROCHA; Tel: +55-91-999828050; E-mail: otavio.rocha@ifpa.edu.br
DOI: 10.1016/S1003-6326(20)65237-2

strength and making them wear-resistant, respectively. This has attracted the interest for the researches that aim to evaluate the influence of these elements on the microstructure and mechanical properties of the multi-component Al−Ni−(Cu/Bi) alloys [9,10].

Due to the requirements for materials under the conditions imposed by motor power systems of higher power, aluminum alloys with additions of solutes of lower hardness meeting the desirable characteristics for alloys with applications in bearings became widely used in tribological applications mainly due to the presence of a relatively rigid matrix (aluminum) with dispersed particles containing soft phases (lead, bismuth, tin, indium, etc) [11−19]. However, alloys containing Pb are being gradually eliminated from production processes due to the deleterious liabilities to the environment and human health generated by this heavy metal [12−18]. On the other hand, Bi is a non-toxic metal and exhibits the same solidification microstructure with lead in aluminum alloy, i.e., globules dispersed in the matrix [10,13−18, 20−27], which acts as constituent layers in sliding bearings, thus reducing the weight of these components employed in various industry fields such as the aerospace and automotive industries [28−31]. Several studies have reported that the micro-structural morphology of alloys of monotectic systems, such as Al−Bi system, is closely related to the thermal parameters imposed during the solidification process [13−27], since according to these researches, the morphologies can vary from a completely globular structure, strings of pearl, or fibrous to a cellular or dendritic structure.

FREITAS et al [17] studied the unsteady-state upward directional solidification of monotectic Al−1.2wt.%Pb and Al−3.2wt.%Bi alloys, and found that the microstructural morphology composed of soft phase containing globules dispersed in the matrix of aluminum was favorable to wear resistance. The authors also observed that for both alloys, the interphase spacing influenced the worn volume (V_w). For Al−Pb monotectic alloys, the behavior was similar to that observed by CRUZ et al [19] for Al−Sn alloys, in which larger spacings generated lower V_w values. On the other hand, the Al−Bi alloy presented the same trend with Al−Si alloys studied by CRUZ et al [19], where tribological behavior, in both investigations, has been optimized for lower interphase spacings.

DAI et al [20] and ROSALES et al [21] investigated the effect of the microstructure on the electrical/thermal and mechanical properties of Al−Sn−Bi alloys. According to Ref. [20], by the addition of Sn to the Al−Bi alloy, a microstructure composed of a Bi and Sn eutectic mixture and aluminum globules forms, which gives better electrical and thermal properties, besides reducing the temperature of alloy welding. ROSALES et al [21] showed that addition of Bi in the Al−Sn alloy improved the fracture toughness response, increased the hardness of the alloy by 60% approximately, as well as increased ductility and did not impair the wear resistance of binary Al−Sn alloy.

Investigations have been conducted to evaluate the effects of Bi on microstructural evolution and morphological changes in solidification processes of aluminum-based binary and multi-component alloys [10,23−27]. In the studies of FARAHANY et al [23,24], addition of Bi in Al−wt.7%Si−0.4wt.%Mg alloys refined the plate-type eutectic silicon particles and promoted a change in the morphology of the Mg_2Si intermetallic phases from plate to fibrous, improving the wear resistance. COSTA et al [25,26] performed studies on unsteady-state upward solidified monotectic Al−Bi−Sn alloys and observed that the Bi content did not have a significant effect on the hardness, but a more homogeneous distribution of eutectic Bi/Sn droplets in the microstructure allowed lower V_w values. Recently, REYES et al [27] have developed the upward solidified Al−3.2wt.%Bi−3wt.%Cu alloy and reported that the wear volume decreases with the decrease of the Bi spacings (λ_{Bi}) up to a maximum value of 16 μm.

On the unsteady-state horizontal solidification of the Al−3wt.%Ni−1wt.%Bi alloy [10], the final microstructure has been characterized by a primary phase consisting of an Al-rich matrix (α) with the presence of the following phases between the α-primary phase: $(\alpha)_{eutectic}$+Al_3Ni intermetallic (β) with Bi particles anchored on the β phase. It was noted that smaller Bi droplets were observed for higher growth rate (V_L) and cooling rate (T_R). In addition, both Bi alloying and thermal parameters have influenced the occurrence of a cell-to-dendrite microstructural transition and, in consequence, different microhardness behaviors have been noted.

However, the influence of the thermal and microstructural parameters on wear behavior has not been investigated, leaving a great gap to be filled with knowledge about the concomitant influence of Al-rich primary phase morphologies (cellular/dendritic microstructure) and sizes and distributions of Bi soft droplet and Al_3Ni hard intermetallic particles on the wear resistance of the horizontally solidified Al−3wt.%Ni−1wt.%Bi alloy. In this sense, the main goal of the present work is to elaborate an experimental study capable of establishing an interrelation between the solidification parameters and the wear resistance of the investigated alloy.

2 Experimental

The experiments carried out on the preparation of the investigated alloy, the horizontal solidification, the determination of experimental thermal parameters and the characterization and quantification of the resulting microstructure have been detailed in the previous work of the present authors [10]. Therefore, in this work, we only reported the experimental methodology on the micro-abrasive wear test by rotating-fixed ball developed in the as-cast samples resulting from the solidification process. The wear resistance of the investigated alloy was examined by means of the micro-abrasive mechanisms, which was based on a rotating sphere and placed in contact with a specimen, in the presence or not of an abrasive solution, producing a surface impression and producing a calotte morphology. The calotte-type impression was evaluated qualitatively and quantitatively, generating data that identify the wear resistance of the tested sample [32−37].

Wear tests were obtained on a machine based on studies published in the literatures [17−19,26]. Figure 1 shows a schematic drawing of the wear machine used in this work, which consists of a pendulum system. One of the pendulum arms is the predetermined load and in the other arm the support contains the fixed sample. Before starting the tests, the general structure of the pendulum system was balanced and, after ensuring the contact of the sample with the ball, the machine was activated, promoting the rotation of the sphere on the surface of the tested sample. Four test times (t) were adopted: 7, 14, 21 and 28 min, which corresponded to the sliding distances (S_D) of 207, 413, 620 and 827 m, the same as those employed in other studies [17−19,26]. It is important to highlight that for each group of tests the use of only one sphere was standardized and, in order to avoid the influence of the ball mark (overlapping wear tracks), it has been rotated by approximately 30°. In addition, for each time, in order to avoid any influence of lubricants or abrasives on the results obtained, the surfaces of the ball and the sample were cleaned with ethyl alcohol.

The wear tests have been carried out in the samples corresponding to the resulting ingot from the horizontal solidification of Ref. [10]. It is emphasized that the as-cast samples were drawn from the cross-section to the heat extraction flow, as schematized in Fig. 2, presenting an area of dimensions of 15 mm × 20 mm to allow the contact of the sphere. In order to analyze the highest possible range of cooling rates and microstructural scales, the samples were selected located at the positions (2, 6, 10, 15, 30 and 80 mm from the cooled interface) that allowed to determine the wear resistance for a wide range of variation of

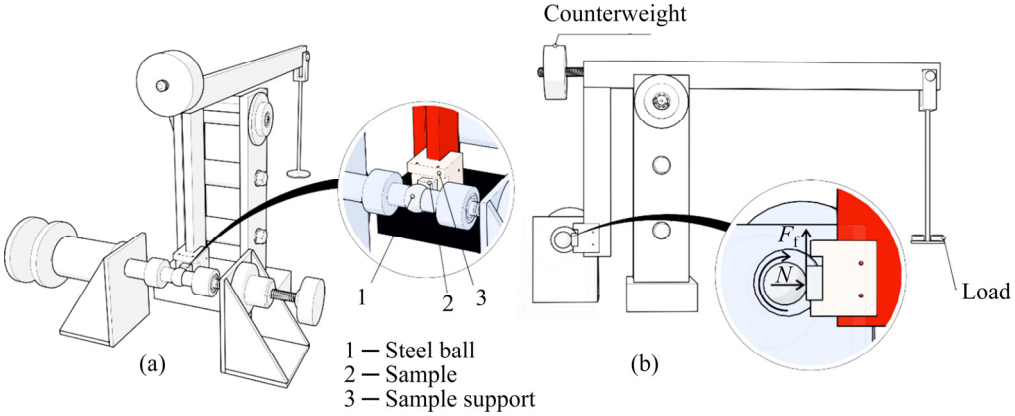

Fig. 1 Schematic representation of wear machine (a) and working loads (b)

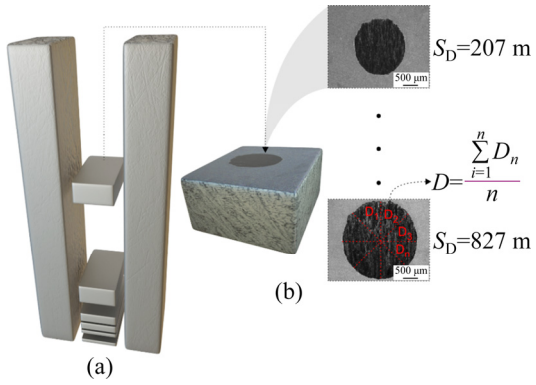

Fig. 2 Specimen removal scheme for wear test (a) and technique employed to measure diameters of ball crater impressions produced by microabrasive wear (b)

interdendritic spacings, diameters and distributions of Bi and Al_3Ni particles.

The used balls in the tests were made of AISI 52100 steel (used in bearings) with a microhardness of HV 850 and a diameter of 25.4 mm. The used ball sliding speed (W) was 0.49 m/s (or W= 370 r/min) and the applied normal contact load was 0.2 N. The tests were carried out under dry sliding friction, that is, in air and under unlubricated conditions to prevent any interfacial element from causing influences on the microstructural features [19,25−27], at 30 °C and a relative humidity of 90%. The spherical wear crater volume (V_w) was calculated according to the Eq. (1) [19,25,26], and the wear rate (R_w), novelty of this work, was calculated according to Eq. (2):

$$V_w = \frac{\pi D^4}{64R} \quad (1)$$

$$R_w = \frac{V_w}{S_D} \quad (2)$$

where D is the worn crater diameter (see Fig. 2(b)), and R is the ball radius. The diameter was measured four times for each worn crater along different radial positions, as indicated in Fig. 2(b). S_D is the sliding distance, which has been calculated by $S_D=W\cdot t\cdot 2\pi R$, and for the four assumed test times, sliding distances were 207, 413, 620 and 827 m, as mentioned before.

A scanning electron microscope (SEM TESCAM, VEGA 3 LMU) coupled to an energy dispersion spectrum (EDS AZTEC ENERGY X-ACT, Oxford) was used during microstructural characterization of as-cast samples and worn crater. Dendritic spacing was measured following techniques from the literatures [10,38−40]. In turn, a SHIMADZU HMV model was used in the microhardnees tests and the adopted Vickers microhardness was the average of at least 20 measurements on each as-cast and heat-treated sample. More information on the experimental procedure and technique used for HV measuring can be observed in our work [10].

3 Results and discussion

Experimental results on thermal analysis, including temperature mapping, thermal parameters (V_L and T_R), and the cellular and primary dendritic spacings (λ_c and λ_1) dependence on V_L and T_R, resulting from the horizontal solidification process of the Al−3wt.%Ni−1wt.%Bi alloy, have been published in our recent investigation [10]. Figures 3 and 4 represent the thermal parameters variation along the length of the horizontally solidified ingot and the effects of the cooling rate on the microstructural evolution. The occurrence of a cell-to-dendrite microstructural transition related to the α(Al) primary phase can be observed: (1) cellular, at positions close to the cooled casting surface, i.e., for higher growth and cooling rates (V_L>0.99 mm/s and T_R>8.8 °C/s) and (2) dendritic, at the positions far from the cooled interface, that is, for lower growth and cooling rates (V_L<0.87 mm/s and T_R<6.3 °C/s).

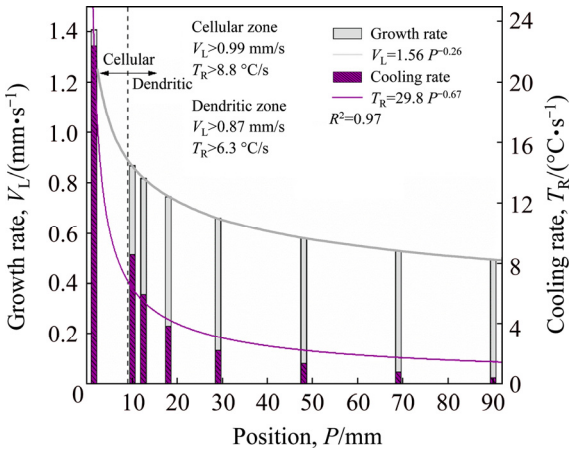

Fig. 3 Change of horizontal solidification thermal parameters as function of position in ingot

The typical solidification microstructure of the investigated alloy is characterized by a primary Al-rich matrix (α) involved by the α(Al)+ Al_3Ni-intermetallic (β) eutectic mixture, with Bi

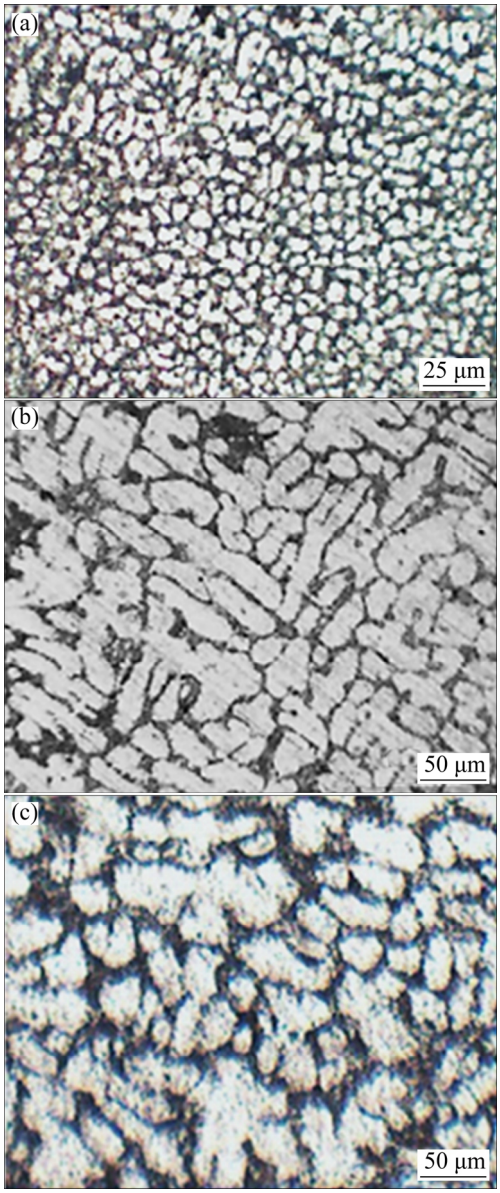

Fig. 4 Microstructural evolution resulting from horizontal solidification of investigated alloy: (a) Cellular (P=2 mm, V_L=130 mm/s, T_R=18.73 °C/s and λ_c=20.38 μm); (b) Dendritic (P=40 mm, V_L=0.60 mm/s, T_R=2.52 °C/s and λ_1=29.61 μm); (c) Dendritic (P=80 mm, V_L=0.50 mm/s, T_R=1.58 °C/s and λ_1=121.19 μm)

particles anchored on the β phase, distributing along the intercellular/interdendritic region. Smaller Bi-droplets and fine rods of fibrous-like β phase are associated with high T_R and V_L values, whereas decreasing the solidification thermal parameters, large Bi-droplets and coarse plates of lamellar-like β phase prevail. Figure 5 shows SEM image with EDS microanalysis for an as-cast sample at position of 50 mm, indicating the eutectic morphologies,

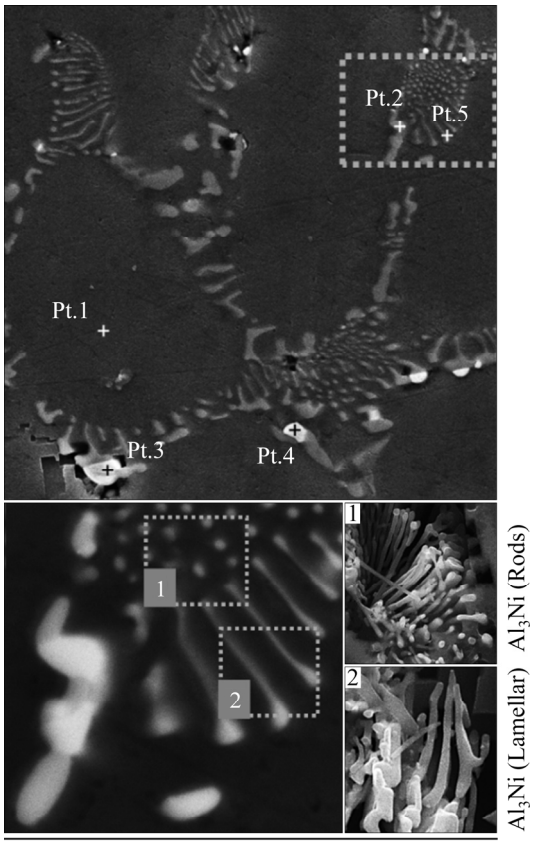

Point	Composition/wt.% (P=50 mm)			
	Al	Fe	Ni	Bi
1	99.30	0	0.07	0
2	74.40	0.4	24.28	0.59
3	1.39	0.17	1.06	97.37
4	7.22	0.05	1.55	91.18
5	90.44	0.16	9.38	0.02

Fig. 5 Typical SEM microstructure with EDS microanalysis, showing morphologies of β-phase and Bi particles

highlighting the Bi globules and globular/rods/lamellar-like Al_3Ni intermetallic compound.

In general, the V_L and T_R variations with the position (P) of the horizontally solidified ingot, as well as λ_1 and λ_c as a function of V_L and T_R, are characterized by mathematical equations given in Table 1.

Figure 6 presents the wear volume (V_w) variation with sliding distance (S_D) for the four test

Table 1 Mathematical equations characterizing thermal and microstructural parameters of studied alloy

Thermal parameter	Microstructural parameter
$V_L=1.56P^{-0.26}$	$\lambda_c=28.3V_L^{-1.1}$, $\lambda_1=50.6V_L^{-1.1}$
$T_R=29.8P^{-0.67}$	$\lambda_c=99T_R^{-0.55}$, $\lambda_1=124.54T_R^{-0.55}$

times and the respective spherical worn craters for two samples of the as-cast ingot from the cooled interface, i.e., P=2 mm and P=30 mm, referring to the cellular and dendritic microstructural regions, respectively. Obviously, the V_w values are higher for larger S_D values (see Fig. 6(a)) and, as a consequence, the size of the worn craters increases with increasing sliding distances, as observed in Fig. 6(b).

3.1 Wear behavior against microstructural evolution

The effects of the microstructure resulting from the horizontal solidification process on the wear resistance of the studied alloy have been investigated and the results are depicted in Figs. 7 and 8. It can be observed that the microstructural scale, parameterized by $\lambda_{c,1}$, has a strong influence on the wear volume (V_w) and wear rate (R_w), with wear behavior presenting better response for lower $\lambda_{c,1}$ values. A variation in wear behavior is identified in the cellular/dendritic microstructural transition zone (MTZ). It is known that the distribution of secondary phases around the matrix (α(Al) primary phase) plays an important role in improving the properties of the materials and is strongly influenced by the morphology of the first solid phase formed. In this sense, the more branched and finer dendritic microstructure induces a better dispersion of the further phases, like β-intermetallic and Bi particles, when compared to the cellular morphology, as can be observed in Fig. 9.

Experimental studies carried out with binary Al−3wt.%Si alloy [19], Al−5wt.%Si alloy [19] and Al−3.2wt.%Bi alloy [17] and with ternary Al−Xwt.%Bi−1wt.%Sn (X=2, 3.2 and 7) alloys [26] report similar wear behavior to those obtained in this study, i.e., V_w increasing with the increase in microstructural scale. For all mentioned alloys, the solute-rich phase formed has higher hardness in comparison to the Al matrix phase, and thus to achieve optimized tribology characteristics, the fine

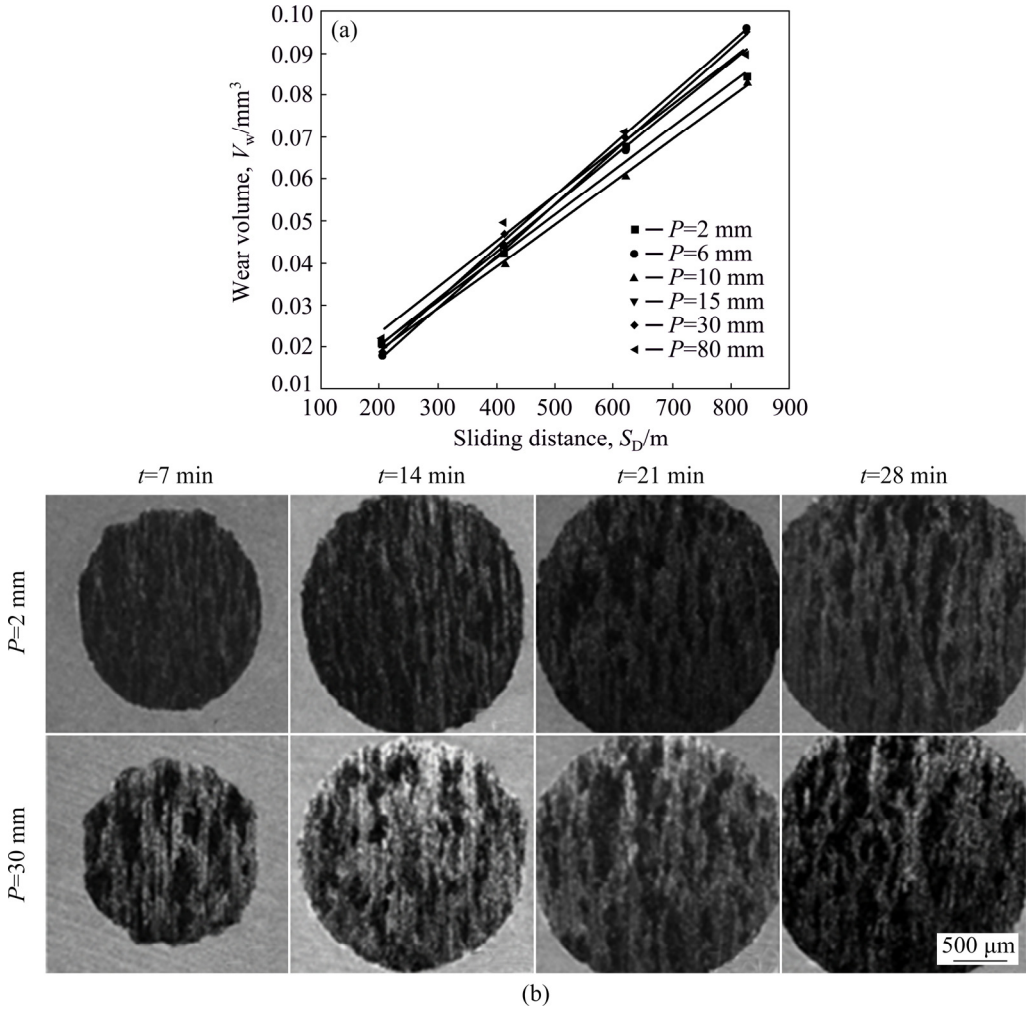

Fig. 6 Wear volume variation with sliding distance (a) and worn craters for four assumed test times (b)

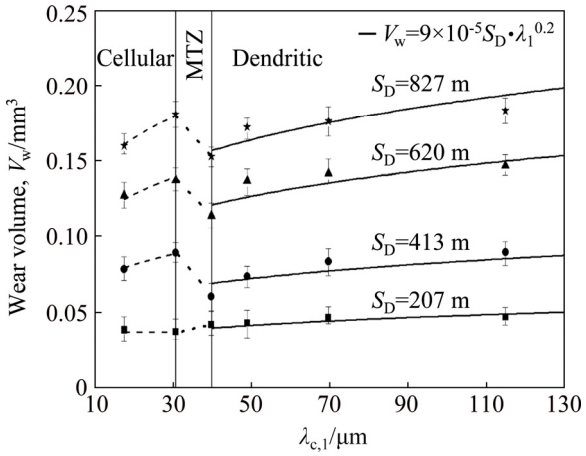

Fig. 7 Wear volume (V_w) as function of cellular or primary dendrite arm spacing ($\lambda_{c,1}$) for different sliding distances (S_D)

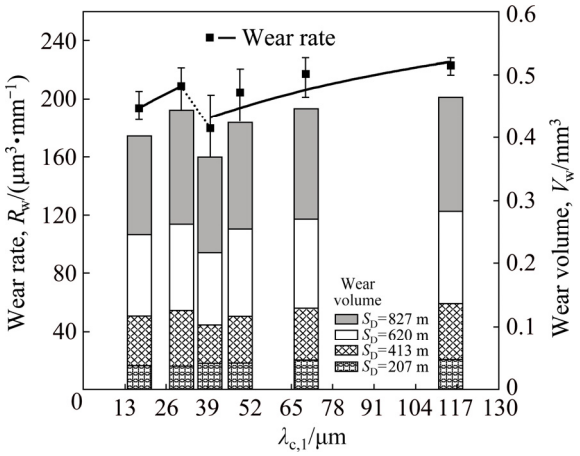

Fig. 8 Wear rate (R_w) and wear volume (V_w) against cellular or primary dendrite arm spacing ($\lambda_{c,1}$)

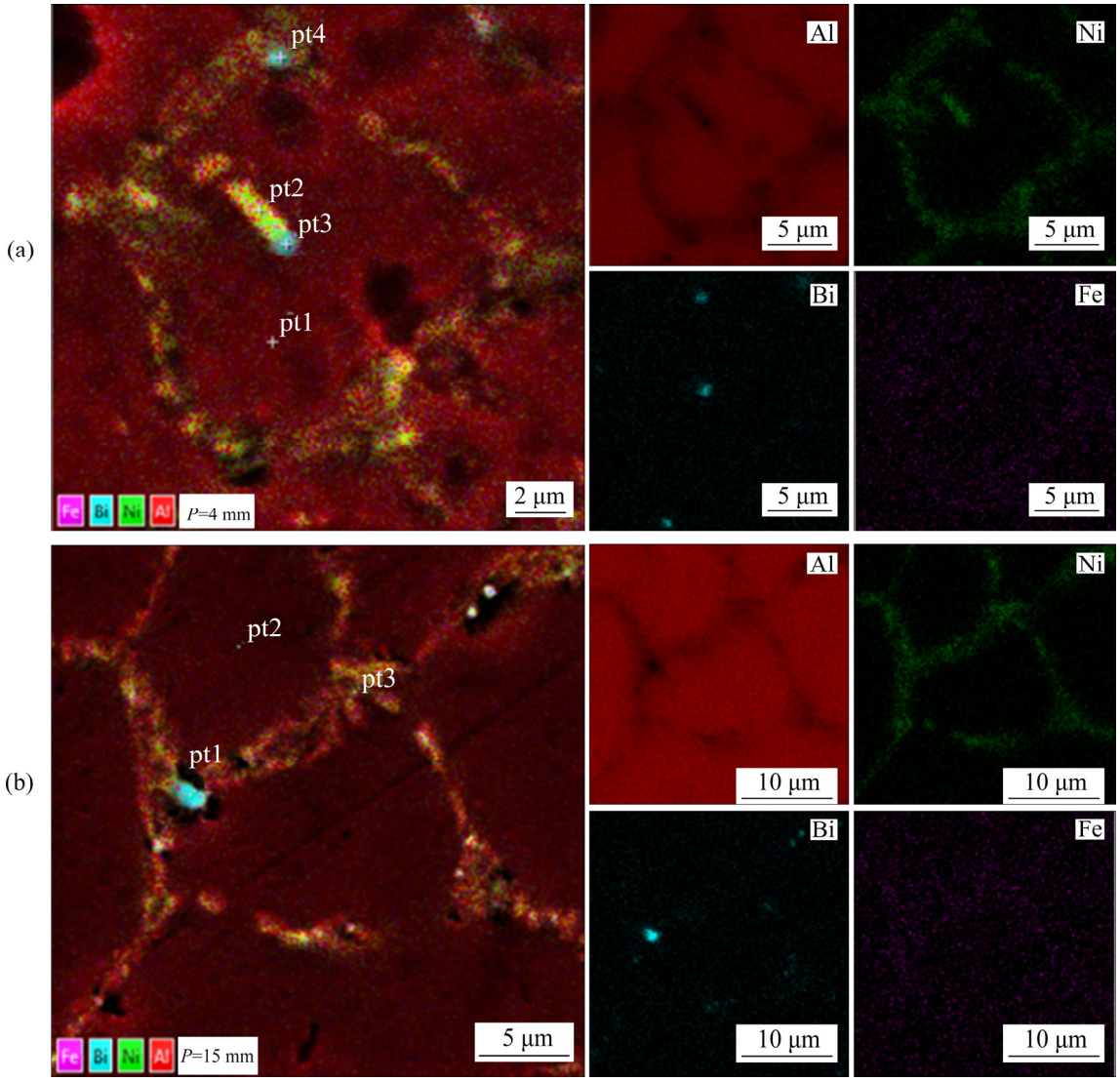

Fig. 9 SEM micrographs and EDS mapping for two samples in ingot from cooled base: (a) P=2 mm, cellular zone; (b) P=15 mm, dendritic zone

and homogeneous distribution of higher-hardness phase is desirable. Specifically for the alloys containing bismuth, FREITAS et al [18] and COSTA et al [26] concluded that the most efficient self-lubricating effect, characteristic of this element, is achieved by a more homogeneous distribution of Bi droplets throughout the microstructure.

Therefore, based on the results found in this work and those reported by the Refs. [17,19,26] for aluminum-based alloys, with the alloying-like Bi element, it is possible to that the best wear resistance, obtained by horizontally solidified Al−3wt.%Ni−1wt.%Bi alloy, was achieved by a finer as-cast microstructure, which provided a better distribution of both hard and soft second phases (β-Al_3Ni intermetallic and Bi droplets, respectively) within interdendritic regions, inheriting at the same time high mechanical strength as well as more effective auto-lubricating effect of the Bi droplets, respectively. Obviously, these results are due to the high cooling rates (0.2−22 °C/s) imposed by the water-cooled solidification process and under transient heat extraction conditions. In general, lower V_w and R_w values are associated with lower λ_c and λ_1 values, as observed in Figs. 7 and 8.

In order to analyze the effect of microhardness (HV) on the wear volume of the investigated alloy, in this work, a relation between V_w versus microhardness has been established, as can be observed in Fig. 10. The results of microhardness were those reported in our study [10]. It can be evidenced that an inverse relationship exists between V_w and microhardness, in both cell and dendritic microstructural regions, since lower V_w values are observed for higher microhardness values, except in the microstructural transition zone (MTZ) where an increase in the dendrite arm spacings is clearly noted during the microstructural transition from cellular to dendritic, as can be verified by the mathematical equations of λ_c and λ_1 as functions of V_L and T_R presented in Table 1. It is in agreement with the literature, since ROCHA et al [39] reported a sharp increase in spacing for Sn−Pb alloys when the microstructure morphology changes from cellular to cellular/dendritic.

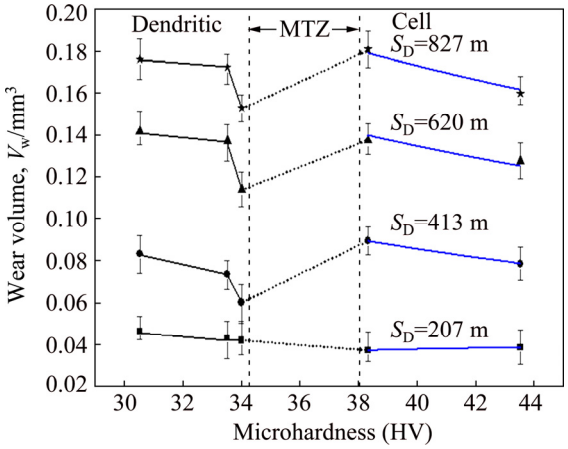

Fig. 10 Relationship between wear volume and microhardness

It is important to highlight that in the dendritic zone the microhardness is independent with the variation of T_R and λ_1, presenting an average value equal to HV 35, while the microhardness values in the cellular zone range from HV 38 to 43, as observed in Fig. 10. Nevertheless, although the cellular region presents combined results of high microhardness value and finer microstructure, lower V_w and R_w values are obtained in dendritic zone. This fact seems to be associated with the lubricating effect of the Bi-droplets, better distributing in the dendritic network and leading to a homogeneous wear condition. In addition, the more branched microstructure acts as a reinforcement to the matrix during mechanical power actions, increasing the overall hardness of the microstructure and consequently improving the wear resistance.

In turn, the slight variation of the worn volume as a function of $\lambda_{c,1}$ for the minor sliding distance tests (S_D=207 m), seems to be related to the short time and insufficient worn material (Bi-droplets) to provide an extensive and continuous lubricating film during the low time wear tests, making the wear behavior practically independent of micro-structural scale under this condition.

3.2 Worn surface and mechanism

Based on DIN 50320 (1979) standard, the wear mechanisms are classified into adhesive wear, abrasive wear, surface fatigue wear, and tribochemical reaction. The adhesive wear was characterized by high wear rate, intense surface damage and large unstable friction coefficient, therefore consisting of severe removing of material, according to STACHOWIAK [37]. Moreover, COSTA et al [26] observed that the effective contact between the counter-body (rolling ball) and the specimen tested provided the adhesion and the material removal, featured by a rough surface in the

worn crater generated by the detachment of material adhered on the counter-body. Conversely, the presence of parallel scratch marks on the worn surface suggests the occurrence of abrasive wear and is related to the presence of harder particles in the tribology system, which penetrates into the surface and generates a furrow as they are forced into and move along the worn surface [33,37]. In this sense, under real conditions, a gradual transition in wear mode is observed as much as the sliding contact remains. Finally, in a recent study of a Bi-containing alloy, the abrasive wear mechanism is introduced after adhesive wear, due to the detachment of agglomerated material (containing lubricant elements) and the subsequent covering of the wear surface [26], increasing the lubricating condition of the worn surface, transiting from adhesive wear to abrasive wear mechanism.

Thus, in order to determine the predominant wear mechanism during the wear tests under assumed conditions on the as-cast samples of the investigated alloy, it is fundamental to analyze the worn surfaces of each specimen tested, providing a detailed overview of the elements which composes the tribology system and influences the wear behavior. For this purpose, all samples tested were examined by scanning electron microscopy (SEM) with EDS mapping/composition microanalysis, and the result for the tested samples is shown in Fig. 11.

In both samples of Fig. 11, the resulting spherical craters of the wear tests can be seen, with an enlarged image indicating two worn regions, which highlight the surface features of the two adhesive and abrasive wear mechanisms observed in all tested samples. For all examined samples of the Al−3wt.%Ni−1wt.%Bi alloy, it is noted that the worn surfaces display regions with severe material detachment, presenting low Bi content (Pt. 2, adhesive wear mechanism region), and sites characterized by parallel scratch marks in the sliding direction, presenting high Bi concentration (Pt. 1, abrasive wear mechanism region). It is

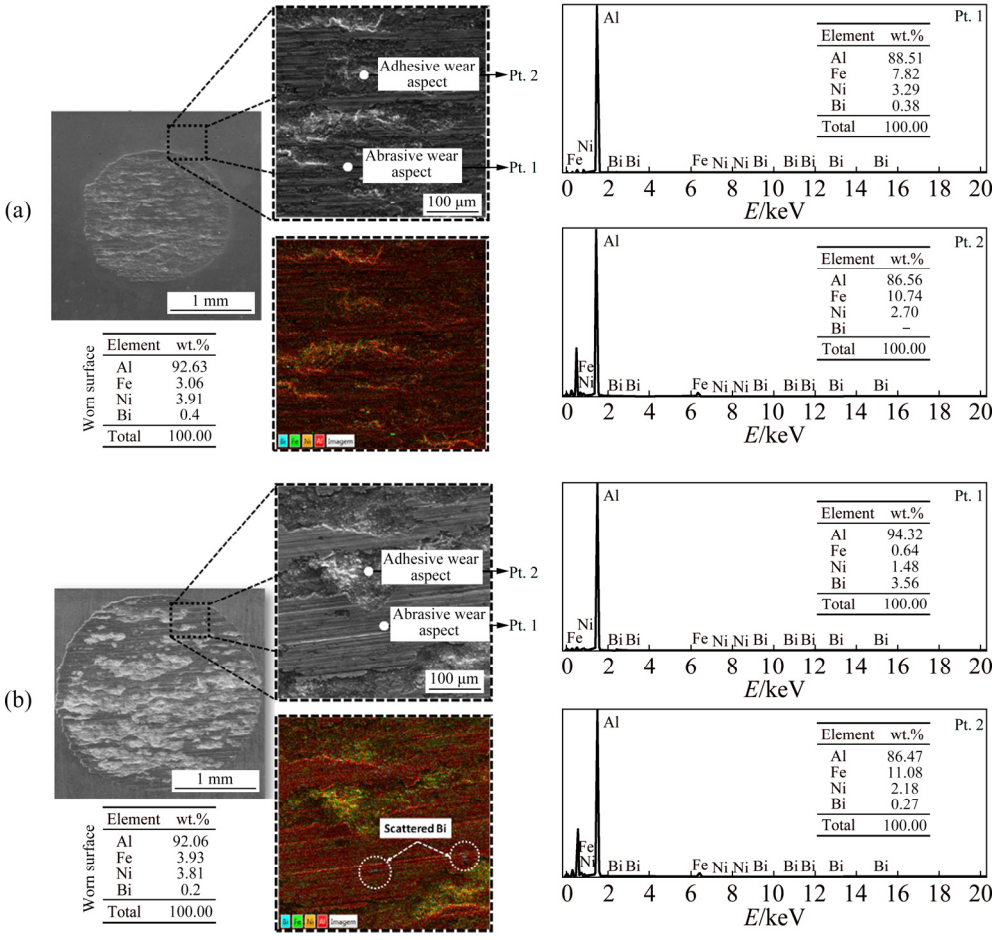

Fig. 11 Worn craters featured with EDS mapping and composition microanalysis, performed on crater surfaces and within typical regions of adhesive and abrasive wear mechanisms, for two positions from cooled interface: (a) P=2 mm; (b) P=80 mm

known that for micro-adhesive wear tests, the major presence of the rough-detached sites inside the crater surface reveals an aggressive wear mechanism, associated with an inefficient lubrication [17,19,26,27,41]. In fact, during the micro-abrasive wear tests carried out in this work, the initial contact of the rolling ball with the flat sample promotes an adhesion and the detachment of material. For self-lubricated alloys, however, this undesirable effect is reduced as the solid lubricate participates in the tribology system, covering the worn scar and minimizing the effective contact between sliding surfaces, and finally promoting a transition of wear mechanism from adhesive to abrasive. WU et al [41] reported lower wear rates and coefficient of friction of a cast Al−Mg_2Si metal matrix composite with the Bi addition and observed a change in wear mechanisms from the combination of abrasive, adhesive and delamination wear without Bi to light abrasive wear and adhesive wear with 1% Bi added.

It is known that the Bi alloying element acts as a solid lubricant on the friction surface, and so the presence of a certain fraction of this soft element in the tribology system may provide a transition of friction mechanism from adhesive to abrasive. On the other hand, the presence of a higher Fe content observed in the EDS analysis performed inside the typical regions of adhesive wear (Pt. 2 of both Figs. 11(a) and 11(b)), indicates that the Fe has been transferred from the steel ball to the worn surface during wear tests. This fact reveals that the lubricant film is ineffective and the contact between the ball and the investigated alloy phases (α(Al) phase, Al_3Ni-intermetallic and Bi-droplets) occurs. Therefore, as the hardness of the Al_3Ni intermetallic compound is around HV 800 [40,42,43], which is relatively close to that of the spherical bearing 52100 steel ball (HV 850), the presence of Fe with higher content in this region indicates that the detachment of this hard phase and the friction against the ball prevail, featured as adhesive wear mechanism.

REYES et al [27] observed for a ternary Bi-containing alloy that adhesive wear prevails because the surfaces of worn samples have large Bi-droplets spacing and fine and shallow grooves for samples featured by finer microstructure. The results for the alloy Al−3.2wt.%Bi−3wt.%Cu [27] are in line with those obtained in this work, in which the continues formation of oxide layer (specially Al_2O_3) and the debris formed by the detached Al_3Ni (HV 714−841 [40,42]) and Bi phases, acts as a third-body in the tribology system. The easier the removal of hard Al_3Ni particles is, the stronger the abrasive and the more aggressive the breakdown of the Bi lubricant film are. It is important to highlight that the discontinuity in the lubricant layer may provide an effective contact between the sliding surfaces, i.e., the wear process proceeds with the adhesion and a severe material removing. In turn, with the continuity of the wear tests, the fraction of Bi particles increases in the tribology system composed by α(Al) phase, Al_3Ni intermetallic and Bi droplets, as mentioned before. The presence of a higher Bi concentration leads to a formation of a new layer of lubricant film, avoiding the direct contact between the sliding ball and the flat sample, and finally converting the wear mechanism from adhesive to abrasive.

Figure 12 presents the results of quantitative and qualitative microanalysis of Bi composition performed by SEM−EDS on the worn crater surfaces of all tested samples, and Fig. 13 shows, for two S_D values, the inverse correlation existing between the wear rate and the Bi concentration on crater surface. A similar correlation for both the minor and intermediate tested sliding distances (207 and 620 m, respectively) is clearly observed. Moreover, it is observed that in the samples characterized by the cellular microstructural morphology, the Bi concentration on the worn surfaces is generally smaller than that characterized by dendritic morphology. This confirms the better

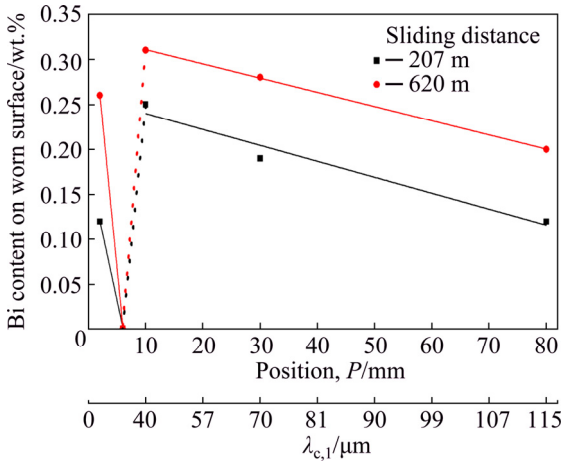

Fig. 12 Average Bi content on worn surface of investigated sample for sliding distances of 207 and 620 m

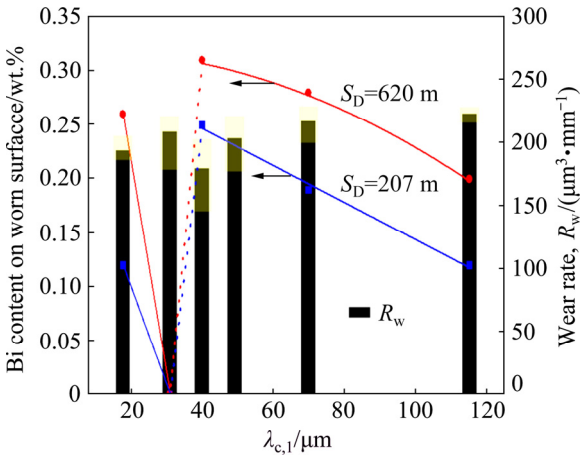

Fig. 13 Average Bi content on worn surface of examined samples against wear rate for sliding distances of 207 and 620 m

distribution and imprisonment of Bi droplets in the dendritic branches, which provides a gradual release of these particles during the tests, favoring the lubricating effect of Bi. In contrast, the unbranched (cellular) microstructure appears to be a non-desirable microstructural mesh for wear resistance purposes, since it provides rapid removal of the Bi droplets present in the intercellular region, depleting and breaking the lubricant layer at the contact between the wear system (ball and as-cast samples).

4 Conclusions

(1) It is observed that for both cellular and dendritic microstructures, the lower V_w and R_w values are reached for higher and lower T_R and $\lambda_{c,1}$ values, respectively. However, cellular and dendritic arrays show different trends, with the latter presenting improved wear resistance.

(2) It is clearly shown that the finer microstructure, due to the high heat extraction rates imposed by the horizontal solidification process, results in an optimized distribution of Bi droplets and Al_3Ni intermetallic and, in consequence, it allows to obtain higher wear resistance for as-cast samples more close to the cooled base.

(3) At the initial moments of wear tests, it is evidenced that the first wear mechanism is the adhesive one, which is dominant and responsible for pulling-out of the hard particles, which are trapped between or on the bodies acting on the tribological system (sample and ball), as well as by the Bi-droplet scattering. Obviously, both soft and hard particles scratch the surfaces of the as-cast samples and, consequently, the abrasive mechanism becomes dominant for the longer wear times. A transition of wear mechanism from adhesive to abrasive is observed.

(4) It is found that the more branched and finer microstructure of the first phase forms during the solidification process, that is, the dendritic microstructure, induces a better dispersion of the other phases, such as the Bi soft droplets and Al_3Ni hard intermetallic particles, when compared to the cellular microstructure. So, lower wear volume and wear rate values in as-cast samples composed of dendritic microstructures are noted.

Acknowledgments

The authors acknowledge the financial support provided by IFPA−Federal Institute of Education, Science and Technology of Pará, UFPA−Federal University of Pará, and CNPq−The Brazilian Research Council (grants 302846/2017-4 and 400634/2016-3), and CAPES−Coordenação de Aperfeiçoamento de Pessoal de Nível Superior−Brasil−Finance Code 001.

References

[1] CANTÉ M V, SPINELLI J E, CHEUNG N, GARCIA A. The correlation between dendritic microstructure and mechanical properties of directionally solidified hypoeutectic Al−Ni alloys [J]. Metals and Materials International, 2010, 16: 39−49.

[2] OSÓRIO W R, PEIXOTO L C, CANTÉ M V, GARCIA A. Microstructure features affecting mechanical properties and corrosion behavior of a hypoeutectic Al−Ni alloy [J]. Materials and Design, 2010, 31: 4485−4489.

[3] ARAUJO I J C, SILVA B L S, SPINELLI J E, GARCIA A. Evolution of eutectic spacing during unidirectional solidification of Al−Ni alloys [J]. Materials Research, 2011, 14: 268−273.

[4] KAYA H, BOYUK U, ÇADIRLI E, MARASLI N. Unidirectional solidification of aluminium−nickel eutectic alloy [J]. Kovove Materialy, 2010, 48: 291−300.

[5] KAYA H, BOYUK U, ÇADIRLI E, MARASLI N. Measurements of the microhardness, electrical and thermal properties of the Al−Ni eutectic alloy [J]. Materials and Design, 2012, 34: 707−712.

[6] KAYA H, BOYUK U, ÇADIRLI E, MARASLI N. Influence of growth rate on microstructure, microhardness and electrical resistivity of directionally solidified Al−7wt%Ni hypoeutectic alloy [J]. Metals and Materials International, 2014, 19: 39−44.

[7] SILVA B L, ARAUJO I J C, SILVA W S, GOULART P R,

GARCIA A, SPINELLI J E. Correlation between dendrite arm spacing and microhardness during unsteady-state directional solidification of Al−Ni alloys [J]. Philosophical Magazine Letters, 2011, 91: 337−343.

[8] KAKITANI R, REYES R V, GARCIA A, SPINELLI J E, CHEUNG N. Relationship between spacing of eutectic colonies and tensile properties of transient directionally solidified Al−Ni eutectic alloy [J]. Journal of Alloys and Compounds, 2018, 733: 59−68.

[9] RODRIGUES A V, LIMA T S, VIDA T A, BRITO C, GARCIA A, CHEUNG N. Microstructure and tensile/corrosion properties relationships of directionally solidified Al−Cu−Ni alloys [J]. Metals and Materials International, 2018, 24: 1058−1076.

[10] AZEVEDO H M, MACHADO G M, BARBOSA C R, ROCHA F S, COSTA R B, COSTA T A, ROCHA O L. Microstructural development of an AlNiBi alloy and influence of the transient horizontal solidification parameters on microhardness [J]. Metallurgical and Materials Transactions A, 2018, 49: 4722−4734.

[11] LEPPER K, JAMES M, CHASHECHKINA J, RIGNEY D A. Sliding behavior of selected aluminum alloys [J]. Wear, 1997, 203−204: 46−56.

[12] KOPELIOVICH D, SHAPIRO A, SHAGAL V. Aluminum−bismuth bearing alloy and methods for its continuous casting [P]. Google Patents, 2001−08−14.

[13] SILVA A P, SPINELLI J E, MANGELINCK-NOËL N, GARCIA A. Microstructural development during transient directional solidification of hypermonotectic Al−Bi alloys [J]. Materials and Design, 2010, 31: 4584−4591.

[14] SILVA A P, SPINELLI J E, GARCIA A. Microstructural evolution during upward and downward transient directional solidification of hypomonotectic and monotectic Al−Bi alloys [J]. Journal of Alloys and Compounds, 2009, 480: 485−493.

[15] SILVA A P, SPINELLI J E, GARCIA A. Thermal Paramenters and microstructure during transient directional solidification of a monotectic Al−Bi alloy [J]. Journal of Alloys and Compounds, 2009, 475: 347−351.

[16] FREITAS E S, OSÓRIO W R, SPINELLI J E, GARCIA A. Mechanical and corrosion resistances of a Sn−0.7wt.%Cu lead-free solder alloy [J]. Microelectronics Reliability B, 2014, 54: 1392−1400.

[17] FREITAS E S, SILVA A P, SPINELLI J E, CASTELETTI L C, GARCIA A. Inter-relation of microstructural features and dry sliding wear behavior of monotectic Al−Bi and Al−Pb Alloys [J]. Tribology Letters A, 2014, 55: 111−120.

[18] FREITAS E S, SILVA A P, SPINELLI J E, CASTELETTI L C, GARCIA A. Microstructure–wear behavior correlation on a directionally solidified Al−In monotectic alloy [J]. Tribology International, 2013, 66: 182−186.

[19] CRUZ K S, MEZA E S, FERNANDES F A P, QUARESMA J M V, CASTELETTI L C, GARCIA A. Dendritic arm spacing affecting mechanical properties and wear behavior of AlSn and Al−Si alloys directionally solidified under unsteady-state conditions [J]. Metallurgical and Materials Transactions A, 2010, 41: 972−984.

[20] DAI R, ZHANG J F, ZHANG S G, LI J G. Liquid immiscibility and core-shell morphology formation in ternary Al−Bi−Sn alloys [J]. Materials Characterization, 2013, 81: 49−55.

[21] ROSALES I, GONZALEZ-RODRIGUEZ G, GAMA J L, GUARDIAN R. Bismuth effect on the mechanical properties of antifriction Al−Sn alloys [J]. Materials Sciences and Applications, 2014, 5: 330−337.

[22] PRASADA A K, DAS K, MURTY B S, CHAKRABORTY M. Effect of grain refinement on wear properties of Al and Al−7Si alloy [J]. Wear, 2004, 257: 148−153.

[23] FARAHANY S, OURDJINI A, IDRIS M H, THAI L T. Effect of bismuth on the microstructure of unmodified and Sr-modified Al−7%Si−0.4Mg alloy [J]. Transactions of Nonferrous Metals Society of China, 2011, 21: 1455−1464.

[24] FARAHANY S, GHANDVAR H, NORDIN N A, OURDJINI A, IDRIS M H. Effect of primary and eutectic Mg_2Si crystal modifications on the mechanical properties and sliding wear behaviour of an Al−20Mg_2Si−2Cu−xBi composite [J]. Journal of Materials Science and Technology, 2016, 32: 1083−1097.

[25] COSTA T, FREITAS E S, DIAS M, BRITO C, CHEUNG N, GARCIA A. Monotectic Al−Bi−Sn alloys directionally solidified: Effects of Bi content, growth rate and cooling rate on the microstructural evolution and hardness [J]. Journal of Alloys and Compounds, 2015, 653: 243−254.

[26] COSTA T A, DIAS M, FREITAS E S, CASTELETTI L C, GARCIA A. The effect of microstructure length scale on dry sliding wear behaviour of monotectic Al−Bi−Sn alloys [J]. Journal of Alloys and Compounds, 2016, 689: 767−776.

[27] REYES R V, PINOTTI V E, AFONSO C R M, CASTELETTI L C, GARCIA A, SPINELLI J E. Processing, as-cast microstructure and wear characteristics of a monotectic Al−Bi−Cu alloy [J]. Journal of Materials Engineering and Performance, 2019, 28: 1201−1212.

[28] POULADVAND S, TAGHIABADI R, SHAHRIYARI F. Investigation of the tribological properties of AlxSi−1.2Fe(Mn) (x=5−13 wt.%) alloys [J]. Journal of Materials Engineering and Performance, 2018, 27: 2223−3334.

[29] KAMIO A, TEZUKA H, KUMAI S, TAKAHASHI T. Unidirectional solidification structure of Al−In monotectic alloys [J]. Transactions of the Japan Institute of Metals, 1984, 25: 569−574.

[30] RATKE L, MÜLLER A, SEIFERT M, KAPSEROVICH G. Monotectic alloys and their growth morphologies [J]. Materials Science Forum, 2010, 649: 137−142.

[31] PHANIKUMAR G, DUTTA P, GALUN R, CHATTOPADHYAY K. Microstructural evolution during remelting of laser surface alloyed hyper-monotectic Al−Bi alloy [J]. Materials Science and Engineering A, 2004, 371: 91−102.

[32] BLAU J P. Friction, lubrication and wear technology [M]. ASM Handbook, 1995: 20.

[33] ZUM GAHR K H. Microstructure and wear of materials [M]. Tribology Series. Amsterdam, Netherlands: Elsevier Science Publishers, 1972.

[34] ZUM GAHR K H. Abrasive wear of two-phase metallic materials with a coarse microstructure in wear of materials [M]. LUDEMA K C. New York: ASME, 1985: 45−58.

[35] BOWDEN F P, ROWE G W. The adhesion of clean metals [J]. Proceedings of the Royal Society A, 1956, 233:

429−442.
[36] RUTHERFORD K L, HUTCHINGS I M. Theory and application of a micro-scale abrasive wear test [J]. Journal of Testing and Evaluation, 1997, 25: 250−260.
[37] STACHOWIAK G W. Wear materials, mechanisms and practice, tribology in practice series [M]. John Wiley & Sons Ltd., 2006.
[38] ROCHA O L, SIQUEIRA C A, GARCIA A. Cellular spacings in unsteady-state directionally solidified Sn−Pb alloys [J]. Materials Science and Engineering A, 2003, 361: 111−118.
[39] LIMA J O, BARBOSA C R, MAGNO I A B, NASCIMENTO J M, BARROS A S, OLIVEIRA M C, SOUZA F A, ROCHA O L. Microstructural evolution during unsteady-state horizontal solidification of Al−Si−Mg (356) alloy [J]. Transactions of Nonferrous Metals Society of China, 2013, 23: 1532−1542.
[40] CHEN R, SHI Y F, XU Q Y, LIU B C. Effect of cooling rate on solidification parameters and microstructure of Al−7Si−0.3Mg−0.15Fe alloy [J]. Transactions of Nonferrous Metals Society of China, 2014, 24: 1645−1652.
[41] WU X F, ZHANG G A, WU F F. Influence of Bi addition on microstructure and dry sliding wear behaviors of cast Al−Mg_2Si metal matrix composite [J]. Transactions of Nonferrous Metals Society of China, 2013, 23: 1532−1542.
[42] KIM T S, HONG S J, AND LEE B T. Hardness behavior of the partially crystallized amorphous Al86Ni9Mm5 alloys [J]. Materials Science and Engineering A, 2003, 363: 81−85.
[43] KE L, HUANG C, XING L, AND HUANG K. Al−Ni Intermetallic composites produced in situ by friction stir processing [J]. Journal of Alloys and Compounds, 2010, 503: 494−499.

凝固工艺参数对 AlNiBi 合金干滑动磨损行为的影响

T. M. BOTELHO[1], H. M. AZEVEDO[1], G. H. MACHADO[1],
C. R. BARBOSA[1], F. S. ROCHA[1], T. A. COSTA[1], O. L. ROCHA[1,2]

1. Federal Institute of Education, Science and Technology of Pará, IFPA,
Almirante Barroso Avenue 1155, 66093-020 Belém, PA, Brazil;
2. Institute of Technology, Federal University of Pará, UFPA, Augusto Correa Avenue 1, 66075-110 Belém, PA, Brazil

摘　要：对经水平定向凝固制备的 Al−3%Ni−1%Bi 合金(质量分数，%)铸态样品进行微磨料磨损试验，研究凝固热学参数(生长速率(V_L)和冷却速率(T_R))以及显微组织参数(晶胞间距(λ_1)和枝晶间距(λ_c))对合金耐磨性的影响。摩擦学参数为磨损量(V_w)和磨损速率(R_w)。分别利用水冷式水平定向凝固装置和固定旋转式磨球机进行凝固试验和磨损试验。结果表明，具有较细显微组织的样品具有较低的 V_w 和 R_w 值。V_w 和 λ_1 之间的关系可以用实验数学方程表示。Bi 软颗粒和 Al_3Ni 硬金属间化合物颗粒在更细的枝晶间分布较好，因此，具有枝晶组织比具有晶胞组织的铸态样品具有更好的耐磨性，可观察到磨损机理由粘着磨损向磨粒磨损转变。

关键词：非稳态水平凝固；干滑动磨损；晶胞/枝晶间距；显微硬度；Bi 颗粒；Al_3Ni 颗粒

(Edited by Bing YANG)